Experimental Mechanics
DOI 10.1007/s11340-012-9677-2

Investigation of Impact Response of Composites with Projection Moiré Enhancement

B. Gulker · R. Lureau · D. Liu

Received: 27 February 2012 / Accepted: 10 September 2012

Abstract As a method for measuring full-field out-of-plane displacement, projection moiré provides high measuring quality with simple experimental setup. Based on an image processing program developed by Heredia and Patterson, this article presents the implementation of projection moiré in low-velocity impact testing. Results from projection moiré agree reasonably well with those obtained from the commonly used load cell method. In an attempt to better document composite response to impact loading, the possibility of correlating the external out-of-plane displacement measurement with the internal delamination is discussed. The technique is further applied to composites with various microstructures, including laminated, two-dimensional woven and quasi-three-dimensional (Q3D) woven composites. Projection moiré is able to provide some insights of the delamination propagation of the composites under impact loading.

Keywords Projection moire · Impact response · Quasi-three-dimensional weaving · Composite materials

Introduction

Drop-weight impact testers (DWIT), such as the one shown in Fig. 1, are commonly used for studying material and structural performance under low-velocity impact. In this setup, a velocity flag in conjunction with an optical sensor provide the initial impactor velocity. The anti-rebound brake engages after the impactor has rebounded is able to stop the impactor from hitting the specimen a second time. The DWIT utilizes a strain-gage based load cell to measure the contact-impact force history of the object being impact-tested. The force history can be converted into velocity and displacement histories with integrations with respect to time. Associated force-displacement curve and energy absorption history can therefore be identified. Because the load cell only measures force at approximately one point, even the state-of-the-art DWIT is not capable of providing the full-surface out-of-plane deformation of the object being tested. The present study uses projection moiré to measure the impact-induced out-of-plane deformation of composite plates. Since it is a full-field measuring technique, it may provide more information concerning the properties and damage process of the composite under impact loading than is available using a standard DWIT test system alone.

B. Gulker · R. Lureau · D. Liu (✉)
Department of Mechanical Engineering,
Michigan State University,
East Lansing, MI 48824, USA
e-mail: liu@msu.edu

Projection Moiré

Experimental Setup

Several techniques, e.g. Ref. [1–5], have been commonly used for measuring deformation of specimens under dynamic loading. Based on projecting a system of lines, i.e. grating, at some angle θ onto the object under investigation, projection moiré and associated techniques have been commonly studied in experimental mechanics [6–13]. Figure 1 (a) is a schematic of the overall (front) view of the DWIT while Fig. 1(b) shows detailed (side) view of the specimen fixture and the setup for projection moiré.

The moiré grating lines deform due to loading and can be recorded by a high-speed camera. The intensity of the images I can be expressed by the following equation:

$$I(x,y) = A(x,y) + B(x,y)\cos(2\pi f_o x + \phi(x,y)) \quad (1)$$

where A and B represent the background intensity and modulation, respectively. The term f_o is called the carrier

Published online: 03 October 2012

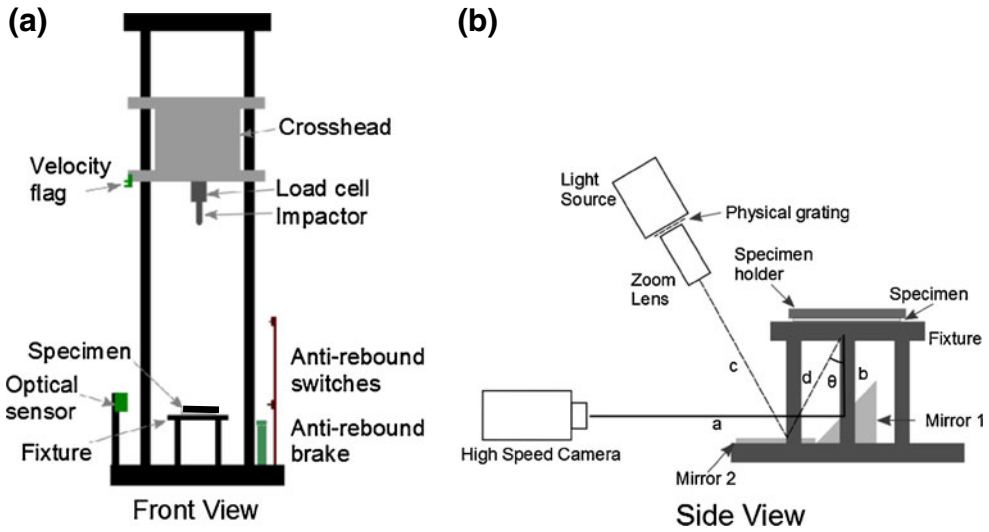

Fig. 1 (**a**) Schematic of the overall (*front*) view of the drop weight impact tester and (**b**) detailed (*side*) view of the setup for specimen and projection moiré

frequency which is related to the grating pitch. The phase ∅ is to be determined by obtaining several intensity maps through virtually shifting the grating and solving the associated system of equations. Since phase is a discontinuous quantity, it must be unwrapped to obtain a continuous quantity in space.

Once the phases at different time steps are identified, the phase difference Δ∅ between a deformed image and the associated reference image can be identified. Accordingly, the out-of-plane displacement related to the deformation between the two images can be found from the following equation:

$$w = \frac{p\Delta\phi}{2\pi \tan\theta} \tag{2}$$

where p is the pitch of the projected moiré grating and θ is the angle between the viewing axis and the projection axis. An angle of 30° was used in the current study.

In implementing projection moiré technique, the concept of infinite optics should be imposed. In application, this requirement may be followed as long as the distance from the camera to the object surface, i.e. the distance combining optical paths *a* and *b* in Fig. 1(b), and the distance from the projector to the object surface, i.e. the distance combining the optical paths *c* and *d* in Fig. 1(b), are at least one order of magnitude higher than the specimen. In this study, both the distances were 750 mm while the effective size of the specimen was 75 mm.

The moiré images were recorded with a high-speed Phantom v12.1 camera and a Zeiss ZF.2 lens. The speed of the recording was between 7,000–15,000 frames/second

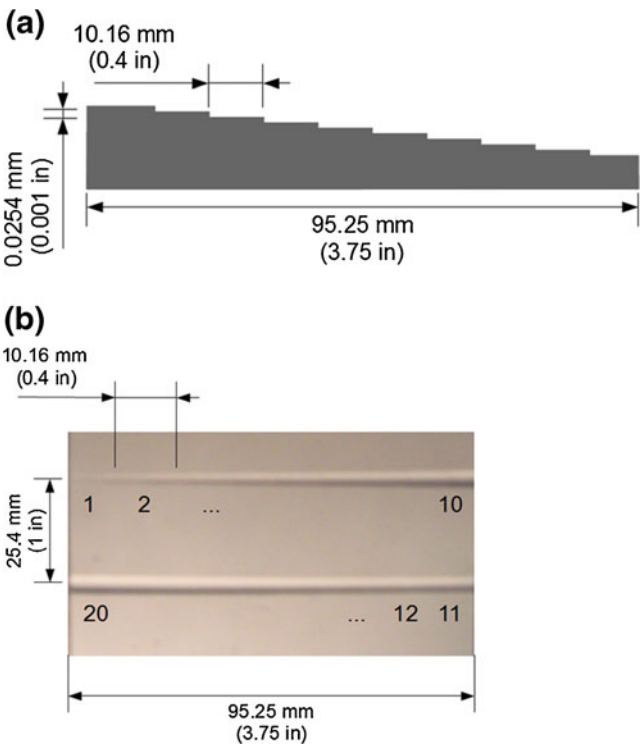

Fig. 2 (**a**) Schematic of the milling steps taken for one notch of the machined aluminum plate and (**b**) image of the calibration plate

Table 1 Standard deviations of various grating densities

Physical Grating: 10 lines/mm	Region 1	0.0389
Projected Grating: 11.74 px/line pair	Region 2	0.0313
	Region 3	0.0302
	All Regions	0.0324
Physical Grating: 20 lines/mm	Region 1	0.0199
Projected Grating: 6.91 px/line pair	Region 2	0.0189
	Region 3	0.0236
	All Regions	0.0214
Physical Grating: 30 lines/mm	Region 1	0.0423
Projected Grating: 5.82 px/line pair	Region 2	0.0529
	Region 3	0.0842
	All Regions	0.0765

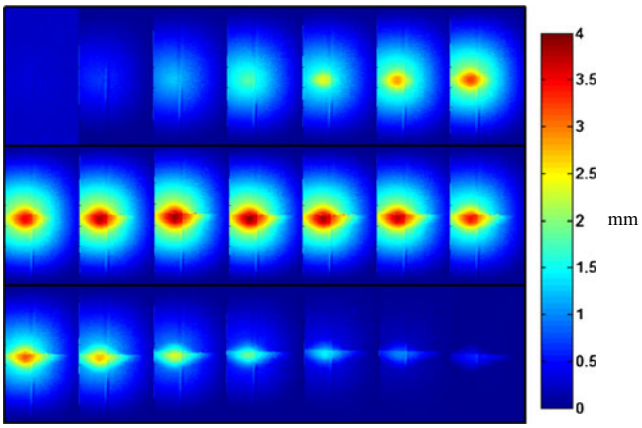

Fig. 3 Deformation contours for evenly spaced time steps (0.33 ms)

depending on the individual tests. Considering that the average impact event for DWIT based tests lasts about 10 ms, this frame rate should provide a sufficient number of data points to capture the physical trends underlined. Since the light sensitivity of high-speed camera decreases as the frame rate increases, the rear surface of the specimen was coated with a white matte paint to maximize the amount of light reflected to the camera, and therefore maximize the frame rate used in the experiments. Additionally, all of the fixture components were painted with a black matte paint to prevent any undesired reflections from contaminating the image. The acquired images were then processed using Heredia-Patterson's image processing program JOSHUA 1.12.2 [13] to determine the out-of-plane deformation.

Calibration Procedures

It is known from Heredia-Patterson's study [13] that the accuracy of the projection moiré method increases as the size of the projected grating decreases. However, the minimum size of projected grating is limited by the resolution of the camera. If the grating is too fine, then there will not be enough pixels to properly represent each grating line. In order to determine the appropriate grating size for use with the projection moiré system, an aluminum plate was machined with two milled notches. Along these notches, the depth of the milling increased in steps incrementally. Initially, the depth was defined as the zero reference. When the mill had traveled laterally for 10.16 mm (0.4 in), the milling depth was increased by 0.025 mm (0.001 in). This was repeated until the edge of the plate was reached. The process was then continued for the second notch. Fig. 2 shows a schematic (a) and image (b) of the calibration plate.

Three different physical gratings were investigated. They were 10, 20 and 30 lines/mm Ronchi rulings. The lens system used to focus the physical gratings onto the specimen also magnified the gratings so that they covered the entire surface of the specimen. Accordingly, the pitches of the three projected gratings on the specimen plane were found to be 0.54, 0.94, and 1.08 lines/mm. Since the resolution of the camera during this test was 1,024 × 1,280 pixels, the pairs of lines of the three projected gratings were hence represented by 11.74, 6.91, and 5.82 pixels, respectively. Calibration tests showed that the standard deviation of the displacement in the flat regions (between the two notched lines of the aluminum plates) was the lowest when there were 6.91 pixels per line-pair. Table 1 shows the comparisons. It then was concluded that 0.94 lines/mm should be used in subsequent tests for the experimental setup.

Additional attention to grating pitch selection is required when implementing projection moiré in dynamic studies. In general, a finer pitch should provide a better result from projection moiré. This is seen in the present study by observing that the standard deviation improved between the 0.54 lines/mm and 0.94 lines/mm tests due to the decrease in grating pitch. However, the resolution of the camera can place a limit on the finest grating allowed. For static applications, cameras have a very high resolution, so it is typically not a problem. For dynamic applications, however, the image resolution reduces significantly because there are fewer pixels available to render each grating line. Therefore, with the finest grating possible, the image would likely appear as a grey blob in the image instead of a system of grating lines. This would

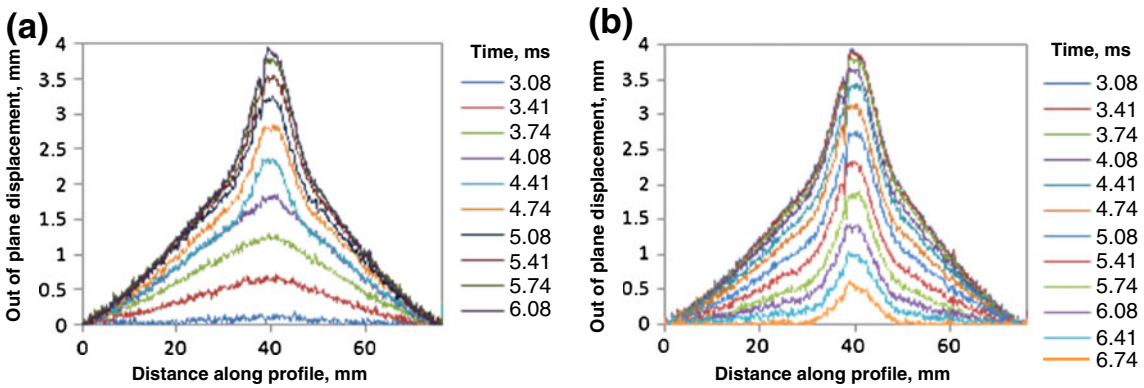

Fig. 4 Profile lines drawn for (**a**) loading and (**b**) unloading histories. The time step between each image is 0.33 ms (Color figure online)

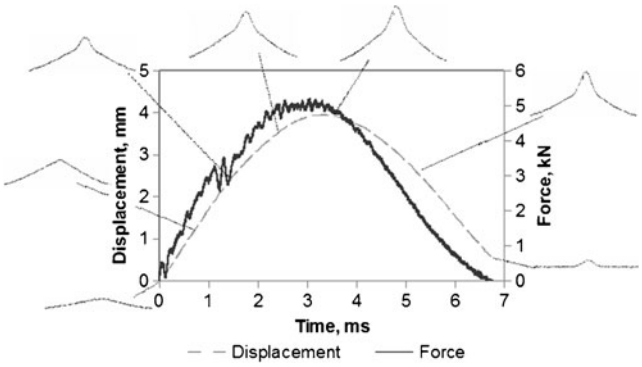

Fig. 5 Force curve from impacted surface and corresponding displacement profiles from non-impacted surface

mean that the image could not be processed for displacement measurement. If the pitch is too fine for the given camera resolution, the grating lines will not be rendered accurately, and the standard deviation will increase. In the present study, the standard deviation became larger between the 0.94 lines/mm and 1.08 lines/mm tests because the camera was no longer able to accurately represent the lines of the projected grating.

Testing Results

A composite material made of E-glass fibers and an epoxy matrix was used to manufacture cross-ply laminates with a thickness of approximately 3.7 mm. All specimens were machined to have dimensions of 125 mm ×125 mm. Each specimen was then sandwiched by two steel plates with a square opening of 75 mm ×75 mm in the center. The square steel-composite set was then held with two bolts along each side before being bolted to the impact testing frame at the four corners. All specimens were impacted at the center. The impacting mass fell from a height of 320 mm and had a mass of 5.16 kg, resulting in an impacting energy of 16.2 J. The force history was recorded by the load cell and the rear surface deflection was recorded by the projection moiré system at a frame rate of 15,000 frames per second. The

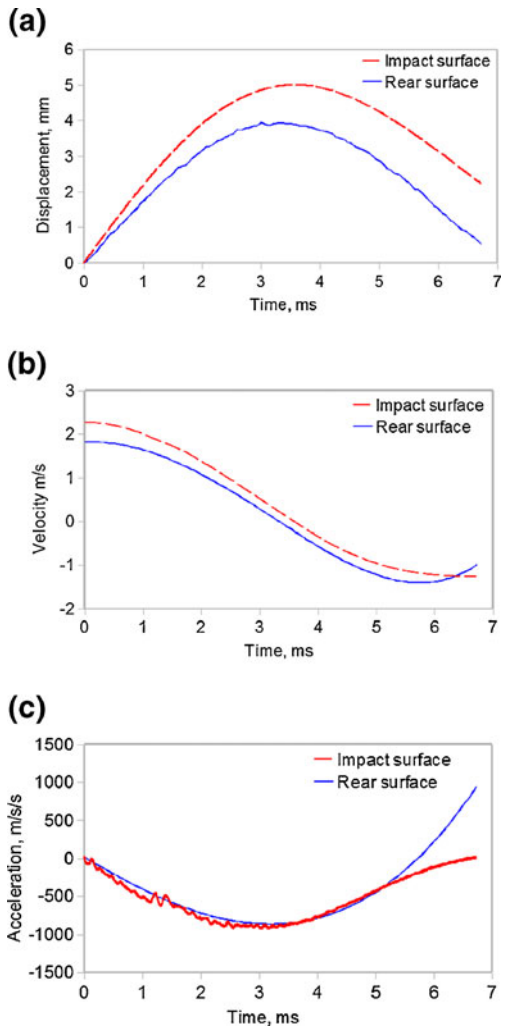

Fig. 6 Comparisons of (**a**) displacement, (**b**) velocity and (**c**) acceleration histories between impacted and rear surfaces at the points of impact (Color figure online)

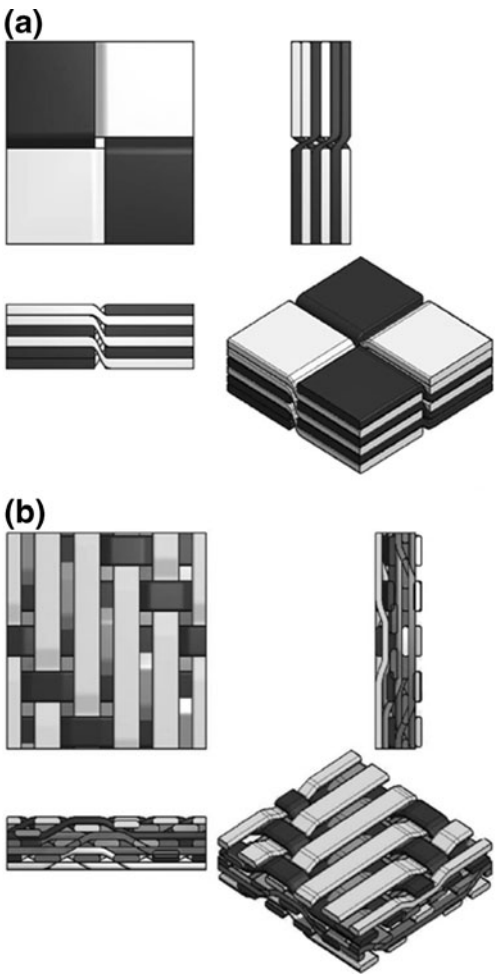

Fig. 7 (**a**) – Quasi-three-dimensional (Q3D) weave. (**b**) – Quasi-three-dimensional five-harness (Q3DO5) weave

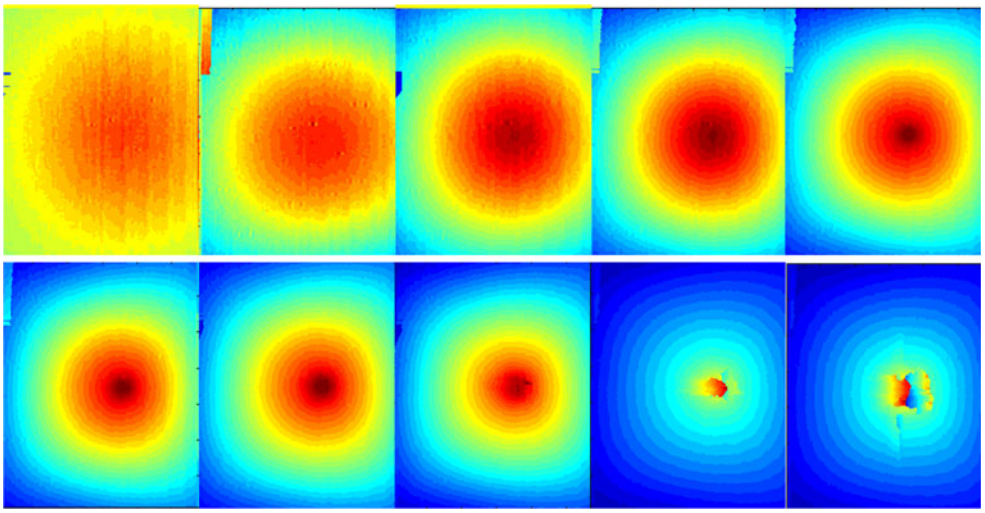

Fig. 8 Deformation contours of Q3D composite with evenly spaced time steps (0.33 ms)

total impact duration for this test was approximately 7 ms, so the impact event was represented by about 100 images. In Fig. 3, 21 evenly spaced images are shown to represent the deformation history. The time step between each frame shown in this figure is 0.33 ms.

Figure 4 shows deformation profiles of the composite plate at different times. Both loading (a) and unloading (b) histories are presented. The time step between each image is 0.33 ms. Each of the deformation profiles in the early loading history looks very much like an isosceles triangle. At some point between 1.08 ms and 1.41 ms, however, the triangular legs stop growing and a large protruded region of 0.6 mm high rapidly forms. After this turning point in the deformation behavior, both the triangular legs and protruded regions grow relatively slowly for the remaining loading history. At the end of loading phase, the protruded region reaches a height of 1.3 mm. Upon unloading, between 3.08 ms and 3.41 ms, both the protruded region and the triangular legs start to decrease. There is some amount of permanent deformation in the protruded region shown in the final deformation profile at 6.74 ms. The final protruded region has a height of 0.6 mm and a width of 18 mm. These two values seem to be comparable with those measured from impacted specimen. Additionally, the off-central line formed by several deformation profiles in Fig. 4(b) matches with the major matrix crack line on the composite surface. It also reflects the sudden change of deformation between the two sides separated by the major matrix crack line on the composite specimen. By further examining the damaged specimen, it is found that the size of overall delamination, i.e. the outermost delamination boundaries on the interfaces, is close to the silhouette area in the last image of Fig. 3.

Discussion on Delamination Process

Like many optical techniques, projection moiré is a technique for surface measurements. The experimental results from the impact testing of the thin composite specimen, however, seem to offer a possibility of correlating the surface deformation and internal damage. As shown in Fig. 5, deformation profiles of the composite plate at several time steps are compared with the force history measured by the load cell. The occurrence of the protruded region matches quite well with the first major disturbance in the force-time curve. Since delamination has been known as the primary damage mode and grows rapidly in the early stage of impact-induced damage process [14], the initiation of delamination seems to be associated with the rapid growth of the protruded region which also occurs in the early stage of low-velocity impact. Since delamination has also been recognized as able to cause significant structural degradation, such as reduction of bending stiffness [15], delamination should cause some decrease in the force-time curve as shown in Fig. 5. A direct verification for the relationship between the growth of delamination and that of protruded region, however, will require more advanced studies.

As given earlier, the height of the protruded region rapidly grows to 0.6 mm and then reaches a maximum of 1.3 mm at the point of maximum deformation before settling at 0.6 mm by end of the impact process. Hence, it seems likely that the size of delamination ceases to grow any further around the time the maximum deformation has been reached since the maximum deformation may include deformations due to damage such as delamination and elastic bending. Again, a direct correlation between the termination of delamination and the maximum protrusion will require more advanced studies. However, if the development of the protruded region and the delamination can be correlated, the material response to impact loading can be better documented when the projection moiré is included in impact studies. Additionally, the significance of this method can be further demonstrated in determining the energy

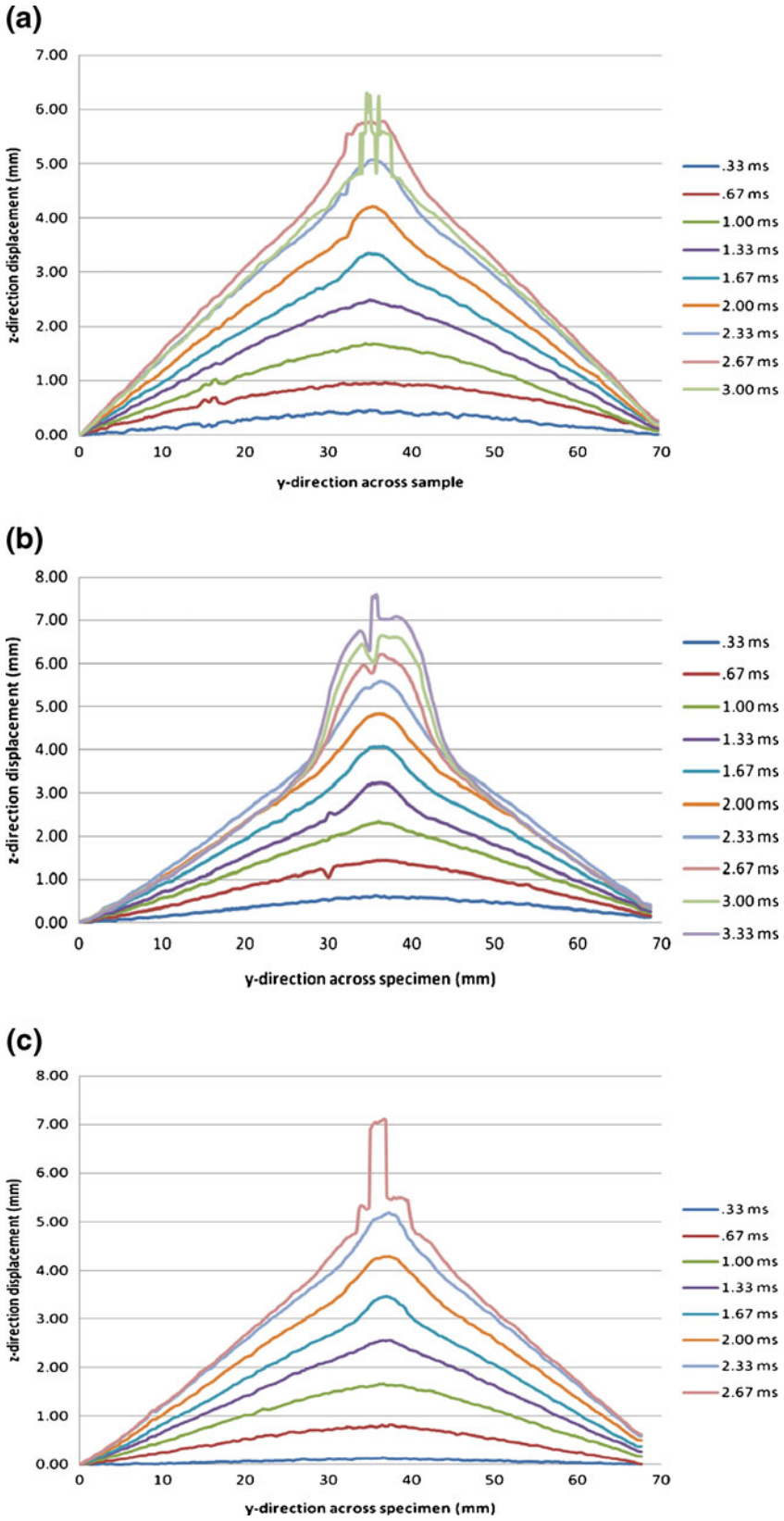

Fig. 9 (**a**) – Out-of-plane displacement profile lines along y-axis for Q3D composite. (**b**) – Out-of-plane displacement profile lines along y-axis for laminated composite. (**c**) – Out-of-plane displacement profile lines along y-axis for 2D composite. (**d**) – Out-of-plane displacement profile lines along y-axis for Q3DO5 composite (Color figure online)

absorbed by a composite plate under impact loading. For example, the rear-layer straining of a woven composite material has been found to be critically important to the impact-induced perforation [15]. Composite materials can be better characterized and compared if projection moiré can be incorporated into the impact investigation.

Fig. 9 (continued)

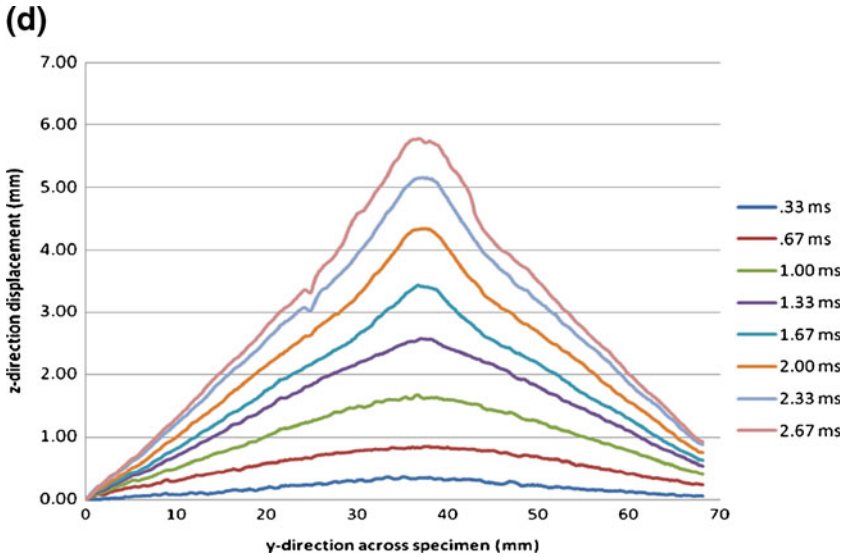

Comparison with DWIT

The results from projection moiré for the rear, non-impacted surface, were compared with the measurements at the impacted surface by the load cell. The load cell provides a measurement of force which is proportional to the acceleration based on the assumption that the impactor is rigid. The acceleration data points were expressed by a polynomial equation. Integration of this equation once provides the velocity history, and a second integration provides the displacement history. This is in contrast to the projection moiré measurement which provides a measurement of out-of-plane displacement. In a similar manner, the displacement data points at the center of the specimen were expressed by a polynomial equation. Differentiation of this equation once provides the velocity history, and a second differentiation provides the acceleration history. The results from the two methods are compared in Fig. 6. The raw data presented here (displacement from projection moiré and force from load cell measurements) were not smoothed. However, one of the effects of performing the calculations (integration and differentiation) performed on the data is that results of the calculation are smooth.

Figure 6(a) shows the displacement histories at the impacted point and the corresponding point at the rear, i.e. non-impacted surface, from both load cell and projection moiré, respectively. Figure 6(b) shows the velocity histories at these two points while Fig. 6(c) shows the acceleration histories at the two points, respectively. It is seen in these figures that the displacement, velocity and acceleration histories from the load cell and those from projection moiré are reasonably close to each other considering that the two measurements were taken on opposite surfaces of the specimen with a thickness of 3.7 mm. It is also noted that the acceleration on the impacted surface is never positive. This is due to the fact that the load cell only measures compressive forces because at the end of each impact event, the impactor separates from the specimen. In order to more fully quantify the reasons for the differences between the quantities, an indentation study on a specimen may be performed with the rear surface unsupported.

Fig. 10 Comparison of load-displacement relations from load-cell (continuous curve) and projection moiré (points)

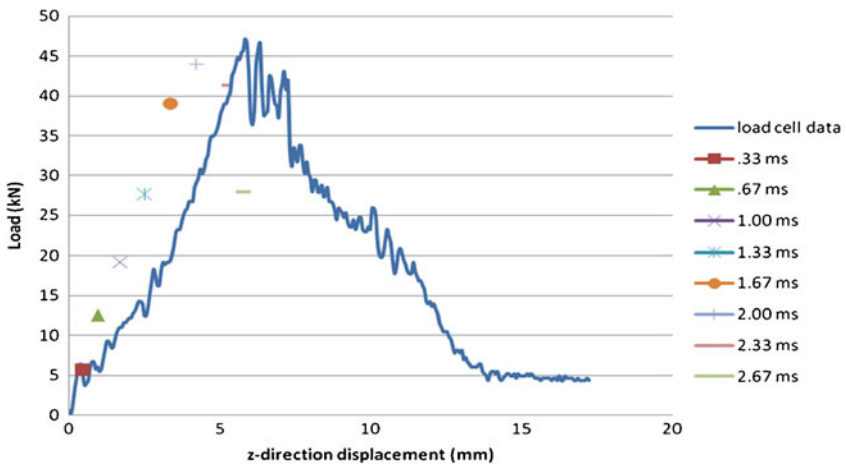

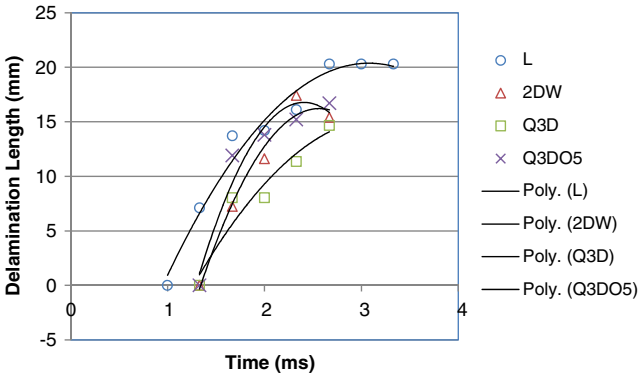

Fig. 11 Initiation and growth of delamination of various composites from projection moiré

Impact Response of Composite Plates

Composite Materials with Various Interlocking

Delamination is a common damage mode in laminated composites. It is associated with the mismatch of material properties between adjacent layers [15]. In a previous study [16], quasi-three-dimensional (Q3D) composites with interlockings of fiber yarns between adjacent layers were found to be superior to laminated composites in resisting impact-induced delamination. In this study, the responses of these composites to impact loading were further investigated with projection moiré enhancement. Four different composite materials were manually prepared. Details of manufacturing procedures can be found in Ref. [16]. They were laminated (L), two-dimensional woven (2DW), quasi-three-dimensional woven (Q3D) and Q3D composite with five harness (Q3DO5). All the composite materials were made from the same E-glass/epoxy prepreg tape. Figure 7(a) shows the details of the microstructure of Q3D composite while Fig. 7 (b) shows those of Q3DO5 composite.

The laminated composite had a stacking sequence of $[0/90]_6$. There was no interlocking between layers. The 2DW was prepared from weaving glass/epoxy strips of 12.7 mm (0.5″) wide into [*0/90*] cross-layers. A total of six cross-layers were then laminated together to form a 2DW composite. In the 2DW composite, the interlocking was only within each layer. The Q3D woven composite also had the orthogonal weaving identical to that of 2DW. However, all adjacent layers were interlocked with one another, resulting in a three-dimensional network through the thickness. Since there was no yarn specifically oriented in the thickness direction as those in the three-dimensional (3D) composites, it was hence called quasi-three-dimensional (Q3D) woven composite. The Q3DO5 composite was similar to the Q3D composite in terms of the interlocking between adjacent layers. However, a five-harness was imposed in the weaving to improve the flatness of the quasi-three-dimensional woven composite. Details of the weaving technique can be found in Ref. [15].

Experimental Results for Q3D Composite

Figure 8 shows the out-of-plane deformation contours of the Q3D composite due to a drop-weight impact. There is a time interval of 0.33 ms between the subsequent contours. The contours were obtained from recording the distorted moiré gratings by a high-speed camera and then processed by the Heredia-Patterson's program [13]. The images in Fig. 8 cover the behavior of the Q3D composite from the beginning of contact-impact until the early stage of perforation during the drop-weight impact event. Based on these images, it is possible to identify the time of perforation (the eighth image) as well as the extent of the damage since the perforation and the associated damage cause irregular, often jagged, contours around the impacting point. The images taken after perforation were deemed unsuitable for deformation analysis due to the significant distortion of the images.

The displacement for each pixel in every image could be identified. The displacement profile lines along the y-direction, i.e. a vertical line through the impacting point, were also identified and shown in Fig. 9(a). The curves represent the out-of-plane displacement of the Q3D composite every 0.33 ms from the beginning of the impact-contact. At 3 ms, the displacement was smaller than that at 2.67 ms. This was because that most of the specimen was still within elastic range except that surrounding the impacting point. Therefore, after the impactor broke through the bottom layer of the composite, the specimen was attempting to recover to its original shape.

In addition to the displacement profile along the y-direction, the out-of-plane displacement history at the impacting point was also constructed. By differentiating the displacement history with respect to time twice and multiplying it with the mass of the impctor, the force-displacement relation for the impact event could be established. It is shown in Fig. 10 along with that obtained directly from the load cell attached to the imapctor. As can be seen, the curve obtained from the load cell and the data points obtained from the projection moiré have a similar shape although the projection moiré gives smaller displacement than the load cell for the same load. This discrepancy was primarily due to the facts that the specimen was compressed and the contact area was varied during impact besides that the measuring locations were on the opposite surfaces of the specimen between the load cell (on the contact surface) and the projection moiré (on the free surface) and the inaccuracies involved in both experimental techniques.

Comparisons with L, 2D and Q3DO5 Composites

The out-of-plane deformation profile lines along the y-axis for laminated, 2DW and Q3DO5 are also shown in Figs. 9 (b), (c) and (d), respectively. Comparing the profile lines along x-axis (not shown) and y-axis, the laminated composite has a very distinguished protrusion along the y-direction, i.e. a large delamination length along the fiber axis of the non-impacted surface layer. The delamination lengths along the two axes in the 2DW composite are similar and smaller. The Q3DO5 composite has similar orientation-dependent delamination lengths as the Q3D composite although the length along the y-axis is shorter. In order to compare the delamination lengths among the cases more accurately, a quantitative comparison is preferred. This is especially true if the time scale can be included in the comparison. Accordingly, the delamination propagation can be reconstructed with the use of projection moiré.

As mentioned earlier, the protruded zone can be viewed as an indicator of delamination initiation and propagation. Without delamination, the deformation curves should be relatively smooth like the beginning four curves shown in Fig. 8(a). At time 1.67 ms, protrusion becomes apparent in the profile line. Two points defining the protrusion can be identified from each curve and delamination length can be subsequently determined. Figure 11 shows the development of delamination length for the four composites subjected to an identical impacting energy. It is clear that the laminated one has the largest delamination length followed by the Q3DO5 composite and the 2D composite. The Q3D composite has the smallest delamination length.

Besides the delamination length under the same impacting energy, the growing rate of delamination for the four types of composite can also be found from Fig. 10. The laminated composite is found to have the earliest (easiest) delamination initiation than the Q3DO5, 2D and Q3D composites. The Q3D composite can is seen to have the smallest delamination size and growing rate. The interlocking among the adjacent layers does play a significant role in the delamination initiation and propagation.

Summary

It has been established in this study that projection moiré is a useful tool for measuring out-of-plane displacement during plate impact testing. The work done by Heredia and Patterson [13] has streamlined its implementation, and allows for an efficient measurement system. The full-field displacement provided by the rear surface measurements gives a comprehensive evaluation of out-of-plane displacement in thin composite specimens. Through observations of the results obtained in this study and a previous study [14], there is an evidence of correlating the growth of major delamination with the out-of-plane measurement by projection moiré. The initiation of delamination is believed as the cause of the first major disturbance in the force-time curve and the beginning protrusion in the deformation profile. The size of delamination is believed to cease growing any further when the maximum deformation has been reached.

Acknowledgement The authors wish to express their sincere thanks to the financial supports from the Office of Naval Research and the U.S. Army TARDEC.

References

1. Kokidko D, Gee L, Chou SC, Chiang FP (1996) Method for measuring transient out-of-plane deformation during impact. International Journal of Impact Engineering 19:127–133
2. Chai H, Knauss WG, Babcock CD (1983) Observation of damage growth in compressively loaded laminates. Exp Mech 23:329–337
3. Sutton MA, McNiell SR, Helm JD, Chao YJ (2000) Advances in 2-D and 3-D computer vision for shape and deformation measurements. In: Rastogi PK, Inaudi D (eds) Photomechanics, Topics in Applied Physics, vol. 77. Elseiver, Oxford
4. Reu, P.L., van Goethem, D.J., Cordova, T.E. (2009). "Measurement of steel plate perforation tests with digital image correlation," *Proceedings of the SEM Annual Conference*, Paper no. 144.
5. Tiwari, V., Sutton, M.A., Shultis, G., McNeill, S.R., Xu, S., Deng, X., Fourney, L., Bretall, D. (2009). Measuring full-field transient plate deformation using high speed imaging systems and 3D DIC. *Proceedings of the SEM Annual Conference*, Paper no. 206.
6. Su X, Chen W (2001) Fourier transform profilometry: a review. Opt Lasers Eng 35:263–284
7. Zhang Q, Su X, Cao Y, Li Y, Xiang L, Chen W (2005) Optical 3-D shape and deformation measurement of rotating blades using stroboscopic structured illumination. Opt Eng 44:1–7, 113601
8. Su X, Chen W, Zhang Q, Chao Y (2001) Dynamic 3-D shape measurement method based on FTP. Opt Lasers Eng 36:49–64
9. Zhang Q, Su X (2005) High-speed optical measurement for the drumhead vibration. Opt Express 13:3110–3116
10. Paepegem WV, Shulev A, Moentjens A, Harizanova J, Degrieck J, Sainov V (2008) Use of projection Moiré for measuring the instantaneous out-of-plane deflections of composite plates subject to bird strike. Optics and Lasers in Egineering 46:527–534
11. Pan J, Huang PS (2006) Color phase-shifting technique for three dimensional shape measurement. Opt Eng 45:013602-1–013602-9
12. Chan PH, Bryanston-Cross PJ (1995) Spatial phase stepping method of fringe pattern analysis. Opt Lasers Eng 23:343–354
13. Heredia M, Patterson EA (2005) Location and shape measurement using a portable fringe projection system. Exp Mech 45:197–204
14. Liu D (2004) Characterization of impact properties and damage process of glass/epoxy composite laminates. J Compos Mater 38:1425–1442
15. Liu D (1988) Impact-induced Delamination - A View of Material Property Mismatching. J Composite Materials 22(7):674–691
16. Rosario, K., & Liu, D (2010) Assessment of quasi-three-dimensional composites – with discussions on fiber straining and weaving effectiveness. *Journal of Composite Materials*, 44, 2953-2973.